Vibrational properties of quasi-periodic beam structures

A. GLACET[a], A. TANGUY[b], J. RÉTHORÉ[c]

a. LaMCoS, Université de Lyon / INSA Lyon / CNRS UMR 5259, arthur.glacet@insa-lyon.fr
b. LaMCoS, Université de Lyon / INSA Lyon / CNRS UMR 5259, anne.tanguy@insa-lyon.fr
c. Research Intitute in Civil and Mechanical Engineering (GeM) CNRS UMR 6183 CNRS / Ecole Centrale de Nantes / Université de Nantes, Julien.rethore@ec-nantes.fr

Abstract :

Quasi-periodic structures have been widely studied, notably in the atomic vibration domain. In this paper a beam structure based on Octohedric quasi-periodic Penrose lattice is studied. We provide a complete description of its vibrational response, including its density of vibrational states, detailed description of its vibration modes, and computation of the dynamical structure factor for transverse and for longitudinal waves. It is shown that quasi-periodic structures exhibit localized low frequency vibration modes that are due to vibrations of isolated patterns in the quasi-periodic structure ; but in opposite high-frequency modes are (non-trivially) extended. Moreover, the paper shows the possible existence of band gaps in the vibrational response of periodic and quasi periodic beam lattices as a function of the ratio between the bending and the tensile stiffness.

Key Words : Quasi-Periodic , Band Gap , Vibration , Beam Lattice

1 Introduction

Quasi-periodic structures have been widely studied for its atomic dynamics, Photonic, magnetic and electronic wave propagation([1], [21], [19]). These structures exhibit complex vibrational behavoiur, including a set of frequency ranges in which no propagative wave exist([3] and [10]), *i.e.* band gaps. Band gaps can lead to interesting applications in various domains ([11]). The recent progress in the additive manufacturing open new possibilities for using quasi-periodic structures by allowing the printing of complex metamaterials, in a consistent manner. Additive manufactured metamaterials can be designed to exhibit unusual macroscopic behavior due to their internal structure as in ([6] and [8]). Therefore the possibility of creating metamaterials having the same properties than the quasi periodic atomic structures can be highly interesting and allow to get rid of unwanted complex behaviors ([10]). Such metamaterial could create band gap in their vibrational mechanical response while being isotropic regarding elastic or wave propagation for example. Moreover, the macroscopic beam structure offers additional possibilities in terms of large scale interactions, and control parameters for tuning the vibrational properties.
The mechanical and vibrational properties of quasi-periodic and of amorphous structures are related to complex mathematical problems due to the impossibility of periodic simplifications. Therefore, in order to solve these problems, big size matrix problems have to be dealed with. This numerical approach

avoids the necessary simplifications associated to (even highly and recently elaborated) homogeneization tools as in [7], and allows getting insights into possible localized vibrations that are difficult tot take into account in homogeneization procedures. In this paper a beam structure based on a octohedric quasi-periodic Pensore lattice approximant is studied (see Figure.1). The octohedric Penrose tilling is chosen for its ability to create a periodic approximant to the quasi periodic tilling thus allowing the use of periodic boundary conditions as suggested in ([9]).It has been shown in [18] that, for ferromagnetic properties, the approximant with periodic boundary conditions closely mimic the infinite lattice properties. The numerical methods used here for the vibrational study of big systems were inspired from atomic vibration studies and applied to finite elements modelization of large scale complex beam structures. First, the vibrational eigenmodes are computed by exact diagonalization of the dynamical matrix restricted to the beam nodes. Then, Kernel Polynomial Method (KPM) is used to calculate the complete Vibrational Density Of States (VDOS) and the Dynamical Structure Factor (DSF) without the need of exact diagonalization of the dynamical matrix. The KPM method is detailed by [16] and was adapted recently to the study of to the vibrational properties of large-size atomic systems by [5]. We apply it here to large scale beam structures. These methods allow accurate description of the vibrational properties of large scale systems, and thus a better understanding of the vibrational response of quasi-periodic structures.
The paper is organized as follows : first the modelization and numerical methods are explained in Section 2 and 3. These methods are firstly applied on a simple periodic beam structure in Section 4, in order to be validated, and to show the influence of the bending stiffness on the vibrational response. Then in Section 5 the methods are applied on a quasi periodic Penrose approximant and the eigenmodes are studied.

2 Model

The beam structure is described by a Finite Element (FE) modelization based on Euler-Bernoulli beam theory. Each node has 3 degrees of freedom (DF), the two components of the displacement (u_x, u_y) and θ the rotation of the beam section at the node. The dynamical problem can be written with classical matrix equation :

$$[K]\{d\} + [M]\{\ddot{d}\} = \{F\}, \tag{1}$$

where $\{d\}$ is the DF vector containing all DFs of all nodes, $[K]$ the stiffness matrix, $[M]$ the mass matrix and $\{F\}$ the external forces in all directions (F_x , F_y and M_z) for all nodes. F_x and F_y are the components of the external load vector and M_z the torque perpendicular to the structure's plane.

When studying the vibrational response the external forces are zero because the system would be at equilibrium at rest, and the displacement is assumed to be a wave solution. Then

$$\{\ddot{d}\} = -\omega^2\{d\}, \tag{2}$$

where ω is the pulsation of the wave response. Thus the dynamical problem can be written

$$[K]\{d\} = \omega^2[M]\{d\}. \tag{3}$$

The periodic boundary conditions are imposed by modifying the previous equation thus equating the DFs of the homologous nodes.

By denoting $[M] = [L]\,[L]^t$ the problem becomes a classical eigenmodes problem

$$[H]\,\{d'\} = \lambda\{d'\}, \tag{4}$$

with

$$[H] = [L]^{-1}\,[K]\,[L]^{-t}\ ;\ \lambda = \omega^2\ ;\ \{d'\} = [L]^{-1}\,\{d\}\,[L]^{-t}, \tag{5}$$

where $[H]$ is a symmetric positive definite square matrix. This dynamical matrix depends on three parameters :

$$\begin{aligned} &K_v = 12 * \frac{EI}{L^3} \text{ The flexural stiffness.} \\ &K_u = \frac{ES}{L} \text{ The traction/compression stiffness.} \\ &m = \rho SL \text{ the mass of a beam element.} \end{aligned} \tag{6}$$

In these formula E is the Young Modulus, ρ the mass density, L the length of a beam element, S the area of a beam section and I the quadratic moment of a beam section. Later on this paper the ratio $\frac{Kv}{Ku}$ will be used. It is to be noted that this ration depends only on the geometry of the beam cross section and it length.

3 Numerical Methods

The determination of the eigen frequencies and eigen modes from the resolution of Equation 5 is highly computationaly demanding. For this reason, approximate methods that do not require exact resolution of the eigen value problem have been developed [4, 16]. The computation of several quantities like the vibrational density of states and the dynamical structure factor is useful for analyzing the vibrational properties of a material. They are obtained without solving the eigen value problem as detailed bellow.

3.1 Participation ratio

The participation ratio (PR) for a given eigenmode j gives information on the ratio of particles participating in each vibration mode. It was used for example to identify possible localized vibrations in disordered systems [15, 20, 2, 17]. It is defined as :

$$P_r(w_j) = \frac{1}{N}\frac{(\sum_i u_i^2(\omega_j))^2}{\sum_i u_i^4(\omega_j)} \tag{7}$$

where N is the number of nodes in the system, u_i is the displacement vector $u_i = \{ux_i, uy_i\}$ for the ith node and ω_j the pulsation of the jth eigenmode. It means that $P_r = 1/N$ when only one isolated node over N supports the vibration, while $P_r = 1 = 100\%$ in case of uniform translation. In order to calculate this participation ratio, the exact solution of Eq. (3) is needed. The resolution is done using the build in function *eigsn* in Matlab. This can be quite long for big systems.

3.2 Vibrational Density of States

The VDOS corresponds to the density of modes depending on the pulsation. It is defined as :

$$VDOS(\omega) = \frac{1}{3N}\sum_{j=1}^{3N}\delta(\omega-\omega_j) \tag{8}$$

Where δ is the Dirac function. Using the Kernal Polynomial Method (KPM) the VDOS can be obtained without the exact resolution of the eigenvalue problem (4). The KPM allows to compute the VDOS for very large systems [4, 16]. The VDOS is now calculated by :

$$VDOS(\omega) = \frac{4\omega}{3N\omega_{max}^2}\frac{1}{\sqrt{1-\varepsilon^2}}\sum_{k=0}^{K} df_k\mu_k T_k(\varepsilon) \tag{9}$$

Where T_k are Tchebichev polynomials, μ_k are expansion Coefficients, df_k Jackson's damping factors and $\varepsilon = \dfrac{2\omega^2}{\omega_{max}^2} - 1$, k going from 0 to K. The Tchebichev polynomials can be obtained by a recurrence relation or by a trigonometric definition :$T_k(\varepsilon) = cos(k\ arccos(\varepsilon)))$. The bigger the k the closer to the continuous solution $VDOS(\omega)$ will be [16].ω_{max} has to be chosen and is found empirically. Moreover,

$$\mu_k = \frac{1}{R}\sum_{r=1}^{R}(\{d\}_0^r)^t\{d\}_k^r \tag{10}$$

Where $\{d\}_0^r$ are random Gaussian vectors and $\{d\}_k^r$ defined by :

$$\begin{aligned}\{d\}_1^r &= [Ht]\{d\}_0^r \\ \{d\}_k^r &= 2[Ht]\{d\}_{k-1}^r - \{d\}_{k-2}^r\end{aligned} \tag{11}$$

With $[Ht] = \frac{2[H]}{\omega_{max}^2} - I$ in order to obtain eigenvalues in $[-1,1]$. When R is large enough the variability due to the random generation of the $\{d\}_0^r$ can be neglected [4].

3.3 Dynamical Structure Factor

The DSF gives the amplitude of the harmonic waves as a function of q the wave vector and w the pulsation. The DSF can be used to obtain the dispersion law. The DSF is calculated separately for transverse (T) and longitudinal (L) displacement, it is defined by :

$$DSF_L(\omega,q) = \sum_{j=1}^{3N}(\sum_{i=1}^{N} qn.u_i e^{q.N_i})^2\delta(\omega-\omega_j) \tag{12}$$

$$DSF_T(\omega,q) = \sum_{j=1}^{3N}(\sum_{i=1}^{N} qn\wedge u_i e^{q.N_i})^2\delta(\omega-\omega_j) \tag{13}$$

where qn the normalized wave vector and N_i the position vector for the ith nodes. $DSF_L(\omega,q)$ corresponds to the Fourier transform of the longitudinal components of the waves with frequency ω. It is also

a measure of the fluctuations in the density of nodes

$$\begin{aligned} DSF_L(\omega,q) &= \int \exp(-i\omega t)\left\langle(\rho(q,t)-\rho_q).(\rho(-q,t)-\rho_{-q})\right\rangle dt \\ &\approx \int \exp(-i\omega t)\sum_{ij}(q.u_i)(q.u_j)\exp\left(iq.(N_i-N_j)\right)dt \end{aligned}$$

with

$$\rho(q,t)=\int \rho(r,t)\exp(iq.r)dr=\sum_{i=1}^{N}\exp\left(iq.(N_i+u_i(t))\right)\approx\sum_{i=1}^{N}iq.u_i(t)\exp\left(iq.N_i\right) \tag{14}$$

being the spatial Fourier transform of the nodes density $\rho(r,t)$. DSF_L is currently measured by inelastic scattering in atomic systems [12], and DSF_T is it transvers waves counterpart.

The KPM is used once again to calculate the DSFs without exact diagonalization. It is now computed as :

$$DSF_L(\omega,q))=\sum_{k=0}^{K}df_k\mu_k^L(q)T_k(\varepsilon) \tag{15}$$

$$DSF_T(\omega,q)=\sum_{k=0}^{K}df_k\mu_k^T(q)T_k(\varepsilon) \tag{16}$$

With ε as previously defined and :

$$\mu_k^L(q)=<\frac{1}{N}(\sum_{i=1}^{N}qn.u_i^0e^{q.N_i})^2(\sum_{i=1}^{N}qn.u_i^ke^{q.N_i})^2>_r \tag{17}$$

$$\mu_k^T(q)=<\frac{1}{N}(\sum_{i=1}^{N}qn\times u_i^0e^{q.N_i})^2.(\sum_{i=1}^{N}qn\times u_i^ke^{q.N_i})^2>_r, \tag{18}$$

the $<>_r$ notation defining the mean over the R random realizations of the u^0 vector.

3.4 Voronoi Decomposition

The decomposition of the displacement on longitudinal and transverse components compared to the wavevector is ill-defined for non-crystalline samples such as the Penrose tilling ([13]). The new displacement decomposition is based on the Voronoi cells volume variations. The Voronoi cell built around a node is the area containing the points closer to this node than every others. The Transverse displacements will be the displacements that do not modify the Voronoi cells' volume and the Longitudinal are the displacements which do. As in [5], we use the A matrix describing the relative volume variation of the voronoi cell centered on the node i, due to the displacement d_j of node j (translation u_x, u_y and rotation θ) :

$$A_{i,j}=\frac{1}{V_i}\frac{\partial V_i}{\partial d_j} \tag{19}$$

This matrix can be quickly obtained from the geometry of the mesh, the detailed method is described

by [5]. With this definition we obtain the longitudinal and transverse displacements by :

$$\begin{aligned} \{d_\eta\} &= P_\eta\{d\} \; ; \; \eta = L,T \\ P_L &= A^t(AA^t)^{-1}A \\ P_T &= I - A^t(AA^t)^{-1}A \end{aligned} \tag{20}$$

This new decomposition is then injected in the VDOS and the DSF calculation. The VDOS formula (10) for example, becomes :

$$\mu_k^\eta = \frac{1}{R}\sum_r^R (\{d\}_0^r)^t P_\eta \{d\}_k^r \tag{21}$$

4 Role of bending in periodic beam lattice

In order to capture the effect of the bending stiffness of a beam lattice, a simple periodic structure is studied first. The ratio between the tensile stiffness and the bending stiffness is varied in order to observe the influence of the latter on the vibrational response.

4.1 Analytical solution for a periodic lattice

A infinite periodic lattice with a simple squared elementary pattern is considered. The simplicity of this lattice allows the use of periodic boundary conditions on an elementary cell in order to reduce the analysis to one cell. Using those conditions and by choosing the solutions of Equation (3) as : $\{d\} = \{a_d\}exp(i(\omega t + q.r))$, Equation 3 is solved analytically.The values [ω,q] that verify $det(([K] - \omega^2[M])\{d\}) = 0$ are calculated using the *MAPLE* software. Figures 2, 3 and 4 show the analytic solution of the dispersion law for two ratios $\frac{K_v}{K_u}$, namely 0.01, 0.5 and 2. For graphical representation, the dimensionless pulsation ω^{adim} defined as $\omega^{adim} = \omega.\sqrt{\frac{m}{K_u}}$, is used.

For the three cases analyzed herein, three surfaces (ω^{adim} as a function of q_x, q_y) are plotted : two acoustic solutions (in phase vibrations of the nodes : blue and red) and one optical (out of phase vibrations of the nodes : green). For $\frac{K_v}{K_u} = 0.01$ and $\frac{K_v}{K_u} = 0.5$, the green and red surfaces merge at $(\frac{\pi}{L}, \frac{\pi}{L})$ whereas for $\frac{K_v}{K_u} = 2$ the two surfaces are disconnected. This creates a frequency range in which no mode exists. This is called a band gap. It can be shown that the analytic solution used above degenerates for (q_x, q_y) reaching $(\frac{\pi}{L}, \frac{\pi}{L})$ giving a double solution and a single one :

$$\{\sqrt{\frac{210(K_v + K_u)}{43m}}, \sqrt{\frac{10K_v}{m}}\} \tag{22}$$

Using the expression of those solutions the size of the band gap depending on $\frac{K_v}{K_u}$ is :

$$\Delta\omega^{adim} = \sqrt{\frac{m}{Ku}}\left(\sqrt{\frac{10K_v}{m}} - \sqrt{\frac{210(K_v + K_u)}{43m}}\right)^+ \tag{23}$$

It is obtained that below a given ratio $\frac{K_v}{K_u}$, no band gap is obtained whereas above a critical value of 0.9545, the size of the band gap increasing as $\sqrt{\frac{K_v}{K_u}}$ as illustrated in Figure 5.

Optical modes in the periodic beam lattice are transverse. Increasing K_v independently of K_u raises the frequency of optical transverse modes thus creating a band gap. Unfortunately $\frac{Kv}{Ku}$ ration higher than 0.1

can't be geometrically obtained while respecting the slenderness requirements for the euler Bernoulli beam model, thus making impossible to create a band gap in this periodic structure. It may be possible to create a band gap by adjusting the mass distribution of the beam or just with a different periodic structure.

4.2 Numerical calculations

To further analyze the vibrational behaviour of the square lattice, the PR and VDOS are now computed from a numerical solution obtained for a 50×50 cells lattice as presented in Figure 6. The system has $N = 2601$ nodes for $3N$ DFs. Periodic boundary conditions are applied along the boundary of the analyzed domain. For these simulations, the parameters used are $L = 0.01m, K_u = 3.5 \times 10^5 kg.s^{-2}, \rho = 1000kg.m^{-3} E = 1.4 \times 10^9 Pa$, $K_v = 2K_u$, $K_v = 0.5K_u$ and $K_v = 0.01K_u$.

For the three values of $\frac{K_v}{K_u}$, the VDOS and PR are computed following the methodology detailed above. The results are plotted in Figures 8 , 7 and 9. In the latter, *i.e.* for $\frac{K_v}{K_u} = 2$, the creation of the band gap is clearly observed in the VDOS and in the PR. Indeed, for around $\omega^{adim} \approx 4$ that corresponds to our analytical value of ω^{adim} in the band gap, the VDOS vanishes and there is no defined value for the PR as no mode exist for ω^{adim} within the band gap. Conversely, for $\frac{K_v}{K_u} = 0.5$ and $\frac{K_v}{K_u} = 0.01$, the VDOS does not vanish and there is no zone with undefined PR. However, for all three cases , the fluctuations of the VDOS are in close relation with the analytically obtained shape of the surfaces giving the three different roots ω^{adim} as plotted in Figures 3, 2 and 4. Concerning the PR, most of the modes have a PR around 0.6 due to the fact that it is the PR of a spatial cosine to which all the nodes participate. This example shows how the VDOS and the PR can be used to interpret the vibrational behavior of the material and to detect band gaps. As expected, it shows as well, that the additional flexural stiffness in the beam lattice models induces a new kind of optical modes, with the related aperture of a band gap depending on K_v in the vibrational response.

5 Quasi Periodic beam lattice

The methodology is now applied to analyze the behaviour of a quasiperiodic beam lattice. The complexity of quasi periodic structures does not allow the calculation of analytical solutions such as previously. Only numerical results are obtained. All the calculations are run on the 4^{th} approximant of a Penrose lattice shown on figure.1. The system has $N = 8257$ nodes and $3N$ DFs. As previously, periodic boundary conditions are prescribed. The parameters of the model are the same as previously : $L = 0.01m, K_u = 3.5 * \times 10^5 kg.s^{-2}, \rho = 1000kg.m^{-3} E = 1.4 \times 10^9 Pa$. To understand the influence of the flexural component of the beam stiffness, two values of $\frac{K_v}{K_u}$ are considered : 0.01, 0.5 and 2.

For $\frac{K_v}{K_u} = 0.5$, respectively $\frac{K_v}{K_u} = 2$, the VDOS and PR are shown in Figure 11, respectively Figure 12. The VDOS of the quasi periodic tilling considered in this section, shares some similarities with the one computed for the periodic square lattice : for $\frac{K_v}{K_u} = 2$ and $\frac{K_v}{K_u} = 0.5$ there is first a bump in the low frequency range related to the accoustic branches, and after a decrease the VDOS increases again which gives an indication concerning the existence of optical branches. Concerning the PR, whereas for the square lattice there is no clear trend in the evolution of the PR, the quasi-periodic tilling analyzed herein behaves differently. It is observed that the PR follows fluctuations that seem (quite surprisingly) opposite to those of the VDOS for $\frac{K_v}{K_u} = 2$ and $\frac{K_v}{K_u} = 0.5$ but similar for $\frac{K_v}{K_u} = 0.1$ expect around $\omega_{adim} = 0.6$ where a drop of the PR correspond to a peak of VDOS. Consequently, in the frequency ranges with a high density of modes, the latters have the tendency to show localized patterns. Conver-

sely, in the frequency ranges with a low density of modes, the latters show diffuse patterns : especially in the high frequency regime, quasi-crystalline structures do not give rise to localized modes, but a $P_r \approx 0.6$ close to that of plane waves. It can finally be noticed concentrations of modes around certain frequencies, notably in higher frequencies which results in waviness of the VDOS. In order to apprehend how the Penrose lattice vibrates, it can be interesting to look at several modes on specific area of the frequency range. Several modes are plotted for $\frac{K_v}{K_u} = 0.01$ (see Supplementary Material for all the modes). Figures 13 and 14 show highly structured modes where the vibration is localized on a star shaped structure as in Figure 17. These modes, localized on *stars*, are present repeatedly in the two regions where the PR decreases. These modes are localized on specific patterns of the lattice. Figure 16 shows that, in the second decaying region of the PR, another kind of localized mode appears as well : it involves a thin but extended crowned of vibrations. This kind of localization is very surprising and specific of quasi-crystals : it shows large scale vibrations, in the high frequency regime. Finally,a complete set of structures with various sizes is excited along the modes and disordered patterns can also be found as in Figure 15 in a frenquency range where the PR is higher.

In order to test the hypothesis of isolated vibrations of specific patterns in the low frequency regime, that would be decorrelated from the overall environment, the *star* structure has been isolated and its own vibrational modes have been studied. In Figure 18 and 19 the VDOS of the *star* is superposed to the PR of the 4^{th} approximant for two ratio $\frac{K_v}{K_u}$. The frequency range of the peak of the VDOS for the isolated star seems to correspond to the frequency for which this structure drives the modes. This might be the cause of the waviness of the VDOS, the vibrational modes concentrate around the frequencies that excites particular sub-structures. This response again is specific of quasi-crystals, since it shows evidences of the vibration of isolated structures, in the low-frequency regime. In this low-frequency range, extended vibrations are expected in crystals.

For $\frac{K_v}{K_u} = 2$, an additional gap is observed in the VDOS Figure 12 meaning that increasing the bending stiffness strongly impacts the vibrational behavior of the lattice, namely by creating additional band gaps. The evolution of those gaps is also observed thanks to the DSF shown in Figures 20 and 21.The maxima of DSF intensity allow a quick visualization of the dispersion law, but in the case of a quasicrystal, a given frequency w does not correspond to a single wave-vector q. Those figures exhibit a classic dispersion relations for quasi periodic structure as it can be found in [14], [1] and [10] for 1D or 2D quasi periodic lattices. We can observe for example pseudo Bernoulli zones overlapping and repeating at quasi periodic periods. But an additional gap is visible in Fig. 21 for $K_v/K_u = 2$, as can be seen from the extinction of the DSF close to $\omega \approx 4$. This large gap is visible in the dispersion law Figure 21 mainly for longitudinal modes.

6 Conclusion

The vibrational properties of periodic and quasi periodic beam lattices were studied in this paper, as a function of the ratio between bending and tensile stiffness of the beams. The Vibrational Density of States, Participation Ratio and Dynamical Structure Factors for longitudinal as well as for transverse waves have been plotted for different ratio of bending over tensile stiffness. This ratio appears to be a driving parameter for the appearance of a large band gap. It is interesting to note that, contrary to the periodic lattice which has anisotropic effective behavior for elasticity and for wave propagation, the Penrose beam structure, that has a higher level of material symmetry, is an apparent isotropic metamaterial. The creation of band gaps in the numerical simulation is the manifestation of the structure intrinsic

property. Then even if the band gaps are only reached with unrealistic geometries it might be possible to obtain band gaps by adjusting other parameters of the structure (mass distribution, viscosity, etc).

Some low-frequency modes of the quasi periodic lattice seems to be driven by sub-structures within the lattice : indeed, the frequencies of these modes in the quasi-crystal correspond exactly to the frequency of the isolated local structure that appears repeatedly in the vibration mode. Conversely, high-frequency localized modes in the quasi-crystal involve large scale linear structures, suggesting the possibility to isolate large-scale and highly symmetric connected paths in the quasy-cristal. A way to select the vibration modes by the type of structure they excite could allow revealing patterns in PR, VDOS or DSF. For instance it could be interesting to study more accurately and systematically the size of the excited structures depending of the frequency of the modes they appear in, since it could have additional consequences on the dynamics of wave packets transport.

Acknowledgment

Discussions with Remy Mosseri and Marc de Boissieu greatly helped our understanding of the quasi-periodic lattices. Discussion with Y Beltukov is highly acknowledged for the use of the KPM method. The support of CNRS through METAMORPH PEPS project is also gratefully acknowledged.

Références

[1] J. Ashraff and R. Stinchcombe. Dynamic structure factor for the fibonacci-chain quasicrystal. *Physical Review B*, 39(4) :2670, 1989.

[2] J. Bauer, T.-M. Chang, and J. Skinner. Correlation length and inverse-participation-ratio exponents and multifractal structure for anderson localization. *Physical Review B*, 42(13) :8121, 1990.

[3] M. Bayindir, E. Cubukcu, I. Bulu, and E. Ozbay. Photonic band-gap effect, localization, and waveguiding in the two-dimensional penrose lattice. *Physical Review B*, 63(16) :161104, 2001.

[4] Y. Beltukov, C. Fusco, D. Parshin, and A. Tanguy. Boson peak and ioffe-regel criterion in amorphous siliconlike materials : The effect of bond directionality. *Physical Review E*, 93(2) :023006, 2016.

[5] Y. Beltukov, C. Fusco, A. Tanguy, and D. Parshin. Transverse and longitudinal vibrations in amorphous silicon. In *Journal of Physics : Conference Series*, volume 661, page 012056. IOP Publishing, 2016.

[6] T. Bückmann, N. Stenger, M. Kadic, J. Kaschke, A. Frölich, T. Kennerknecht, C. Eberl, M. Thiel, and M. Wegener. Tailored 3d mechanical metamaterials made by dip-in direct-laser-writing optical lithography. *Advanced Materials*, 24(20) :2710–2714, 2012.

[7] C. Chesnais, C. Boutin, and S. Hans. Wave propagation and non-local effects in periodic frame materials : Generalized continuum mechanics. *Mathematics and Mechanics of Solids*, 20(8) :929–958, 2015.

[8] C. Claeys, B. Pluymers, P. Sas, and W. Desmet. Design of a resonant metamaterial based acoustic enclosure. In *Proceedings of the 26th International Conference on Noise and Vibration Engineering, ISMA*, 2014.

[9] M. Duneau. Approximants of quasiperiodic structures generated by the inflation mapping. *Journal of Physics A : Mathematical and General*, 22(21) :4549, 1989.

[10] M. Engel, S. Sonntag, H. Lipp, and H.-R. Trebin. Structure factors of harmonic and anharmonic fibonacci chains by molecular dynamics simulations. *Physical Review B*, 75(14) :144203, 2007.

[11] M. Florescu, S. Torquato, and P. J. Steinhardt. Complete band gaps in two-dimensional photonic quasicrystals. *Physical Review B*, 80(15) :155112, 2009.

[12] V. M. Giordano and G. Monaco. Inelastic x-ray scattering study of liquid ga : Implications for the short-range order. *Physical Review B*, 84(5) :052201, 2011.

[13] J. Hafner and M. Krajčí. Propagating collective excitations in quasi-crystals. *EPL (Europhysics Letters)*, 21(1) :31, 1993.

[14] J. Hafner, M. Krajčí, and M. Mihalkovič. Propagating and localized elementary excitations in decagonal quasicrystals. *Physical review letters*, 76(15) :2738, 1996.

[15] J. M. Larkin. *Vibrational Mode Properties of Disordered Solids from High-Performance Atomistic Simulations and Calculations*. PhD thesis, Citeseer, 2013.

[16] L. Lin, Y. Saad, and C. Yang. Approximating spectral densities of large matrices. *SIAM Review*, 58(1) :34–65, 2016.

[17] P. Sheng and B. van Tiggelen. Introduction to wave scattering, localization and mesoscopic phenomena., 2007.

[18] E. S. Sørensen, M. V. Jarić, and M. Ronchetti. Ising model on penrose lattices : boundary conditions. *Physical Review B*, 44(17) :9271, 1991.

[19] A. Szallas and A. Jagannathan. Spin waves and local magnetizations on the penrose tiling. *Physical Review B*, 77(10) :104427, 2008.

[20] S. Taraskin and S. Elliott. Nature of vibrational excitations in vitreous silica. *Physical Review B*, 56(14) :8605, 1997.

[21] Y. K. Vekilov, I. Gordeev, and E. Isaev. Electronic spectrum of a two-dimensional fibonacci lattice. *Journal of Experimental and Theoretical Physics*, 89(5) :995–999, 1999.

Figures

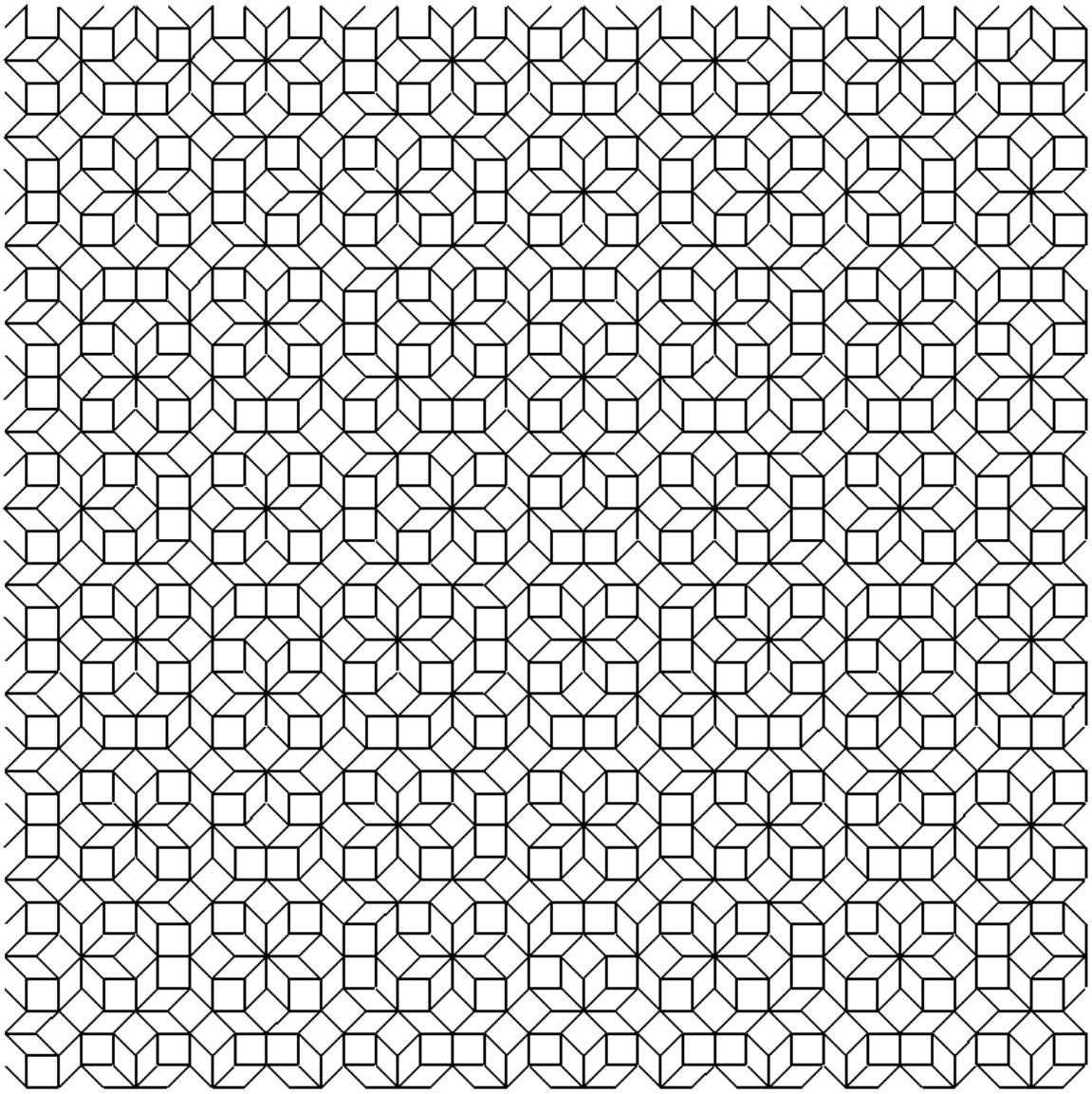

FIGURE 1 – 4th approximant of Penrose tilling beam structure.

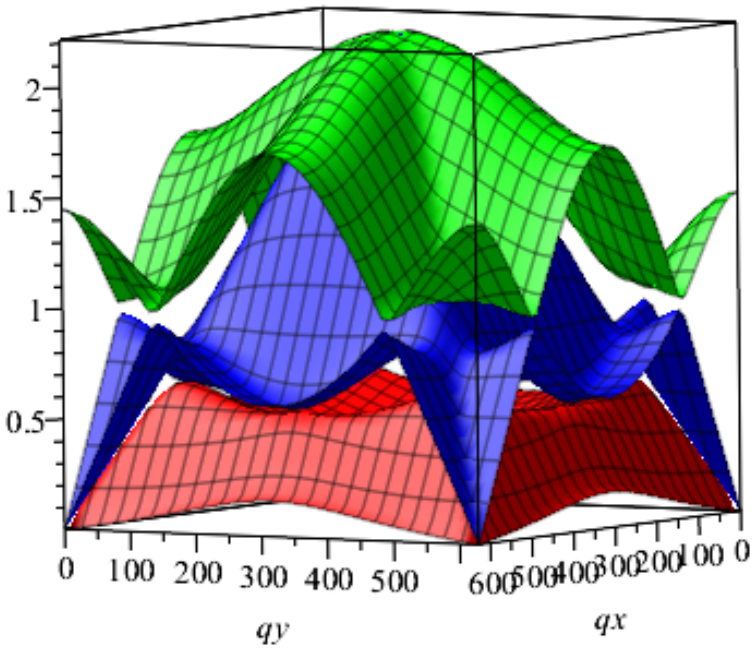

FIGURE 2 – Analytic dispersion relation $\omega_{adim}(q_x, q_y)$ for an infinite Square lattice for $\frac{K_v}{K_u} = 0.01$.

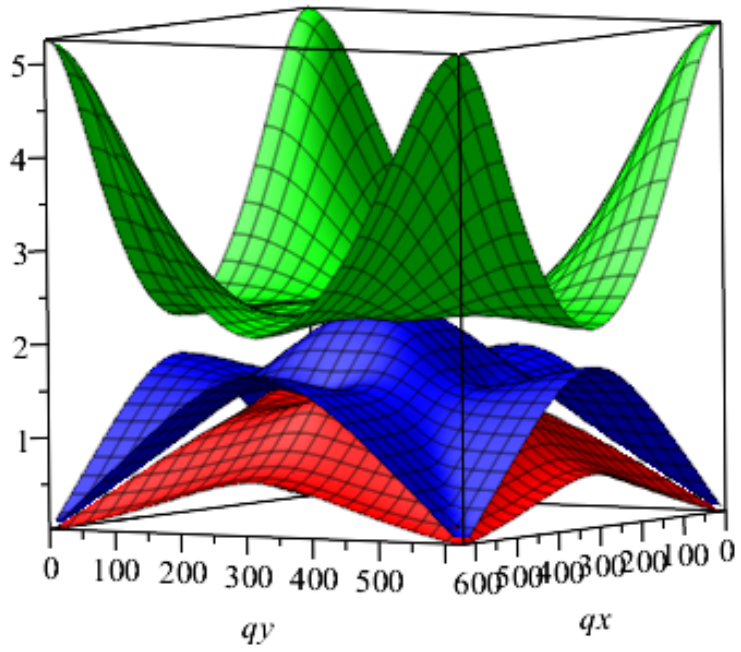

FIGURE 3 – Analytic dispersion relation $\omega_{adim}(q_x, q_y)$ for an infinite Square lattice for $\frac{K_v}{K_u} = 0.5$.

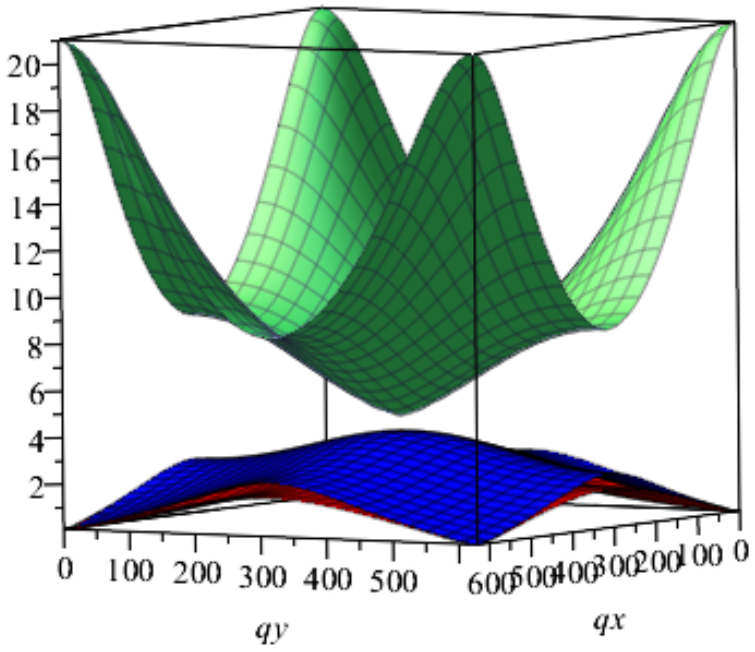

FIGURE 4 – Analytic dispersion relation $\omega_{adim}(q_x, q_y)$ for an infinite Square lattice for $\frac{K_v}{K_u} = 2$.

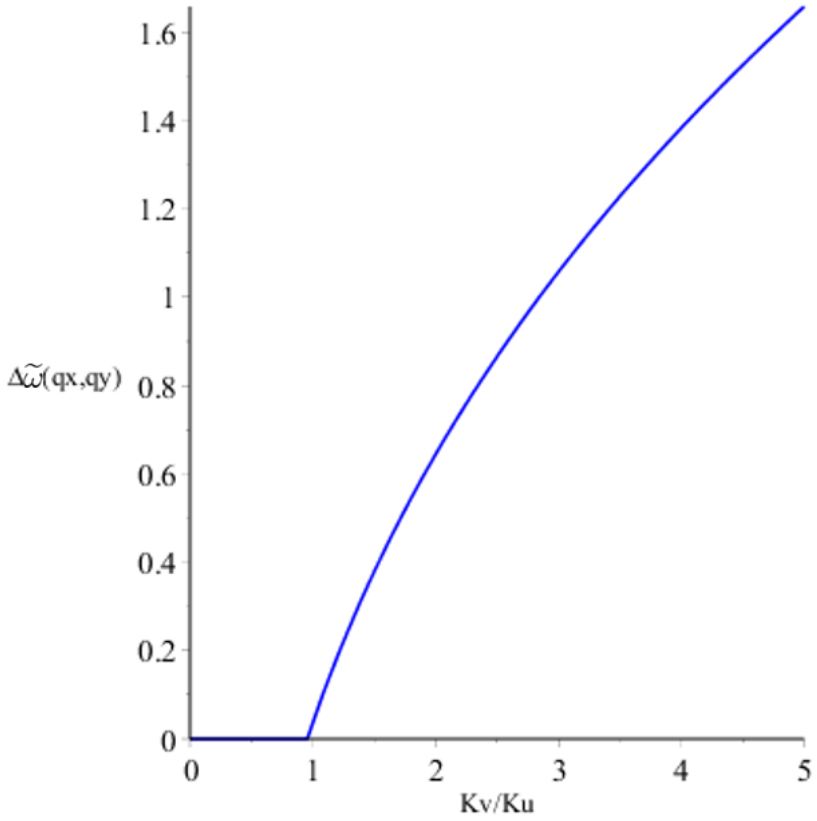

FIGURE 5 – Analytic band gap for an infinite square lattice in function of $\frac{K_v}{K_u}$.

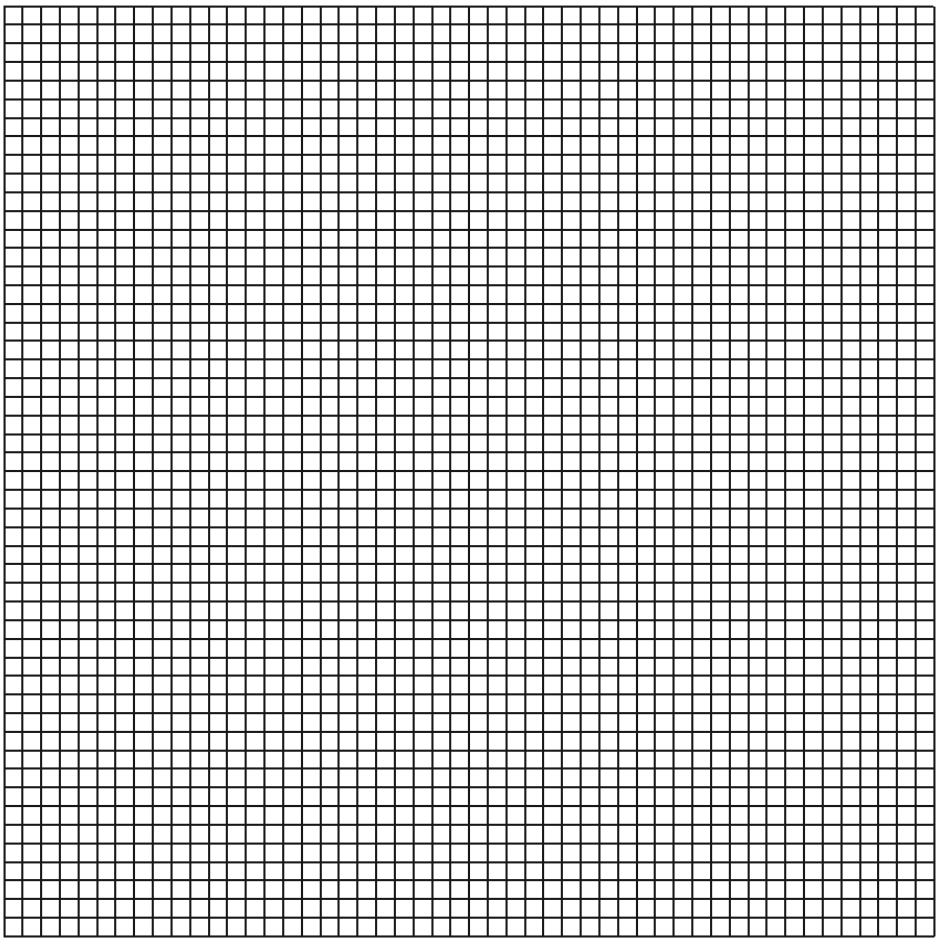

FIGURE 6 – 50×50 square beam structure.

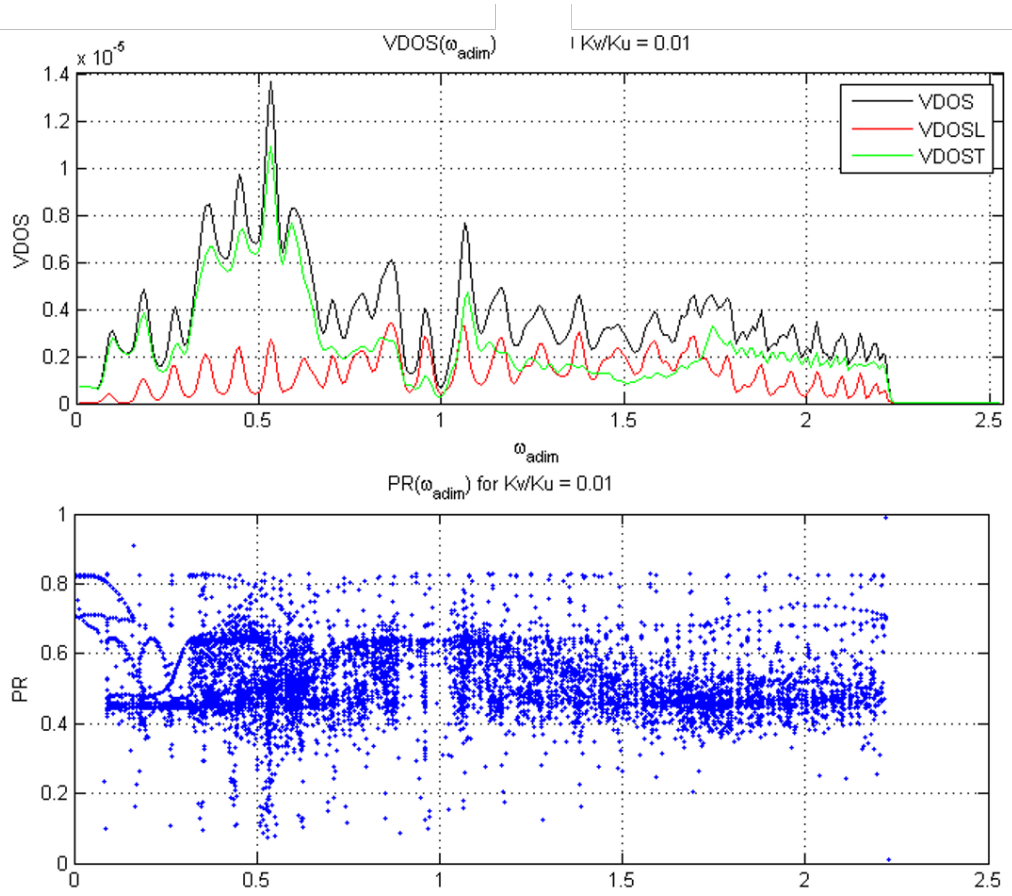

FIGURE 7 – top :Complete, Longitudinal and Transverse VDOS for the 50×50 square lattice with $\frac{K_v}{K_u} = 0.01$. bottom : PR for the same structure.

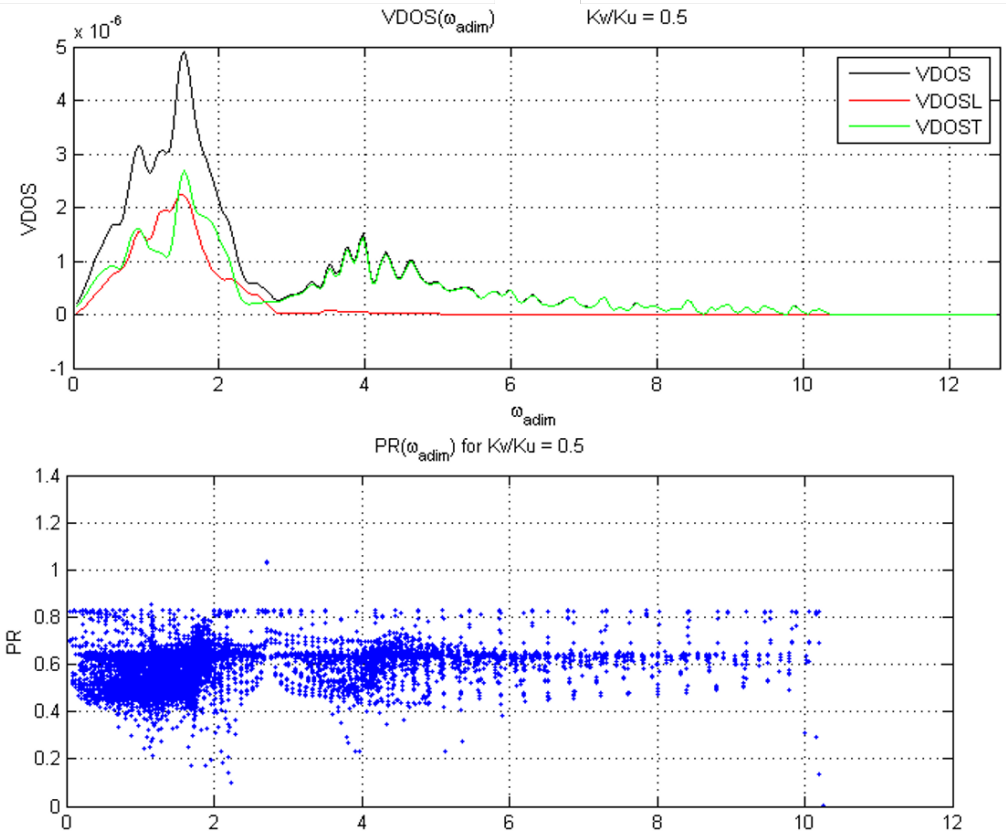

FIGURE 8 – top :Complete, Longitudinal and Transverse VDOS for the 50×50 square lattice with $\frac{K_v}{K_u} = 0.5$. bottom : PR for the same structure.

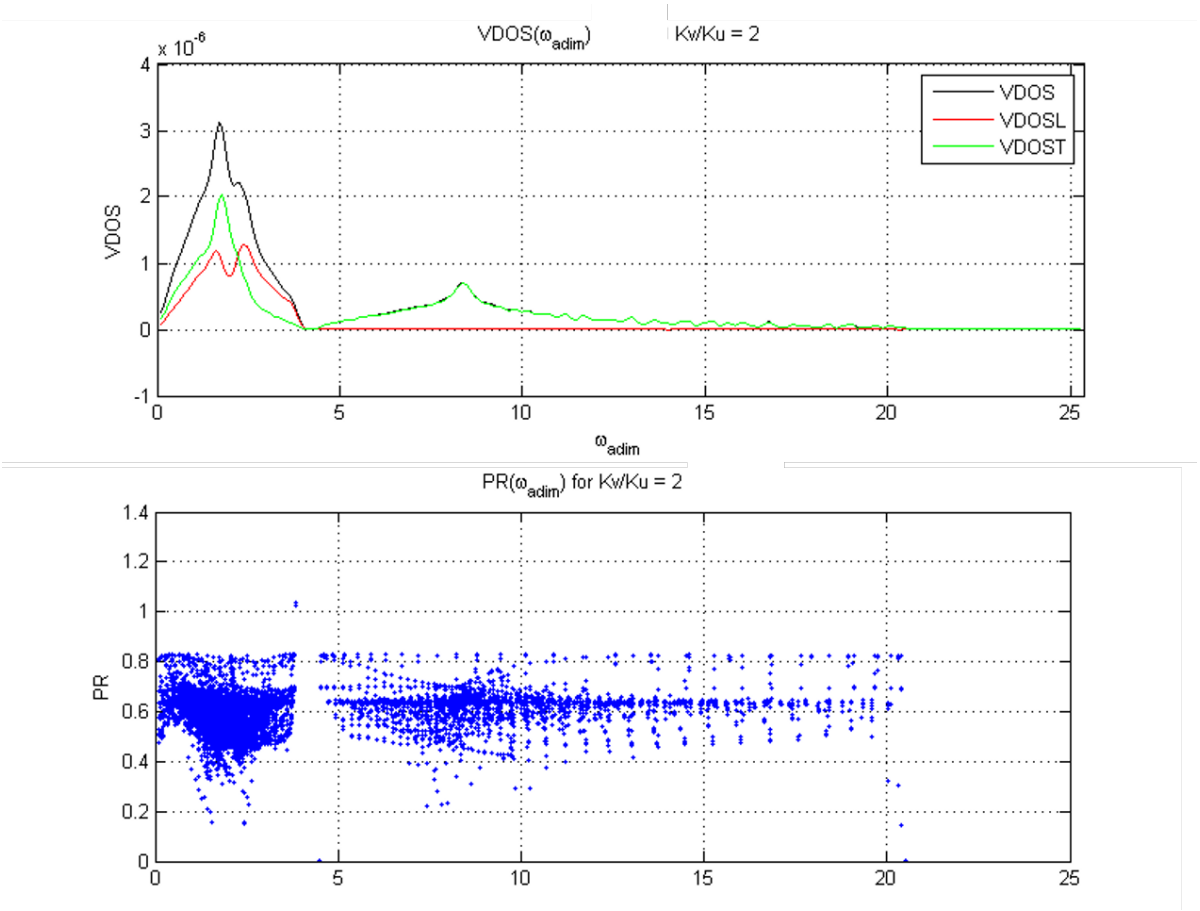

FIGURE 9 – top : Complete, Longitudinal and Transverse VDOS for the 50×50 square lattice with $\frac{K_v}{K_u} = 2$. bottom : PR for the same structure.

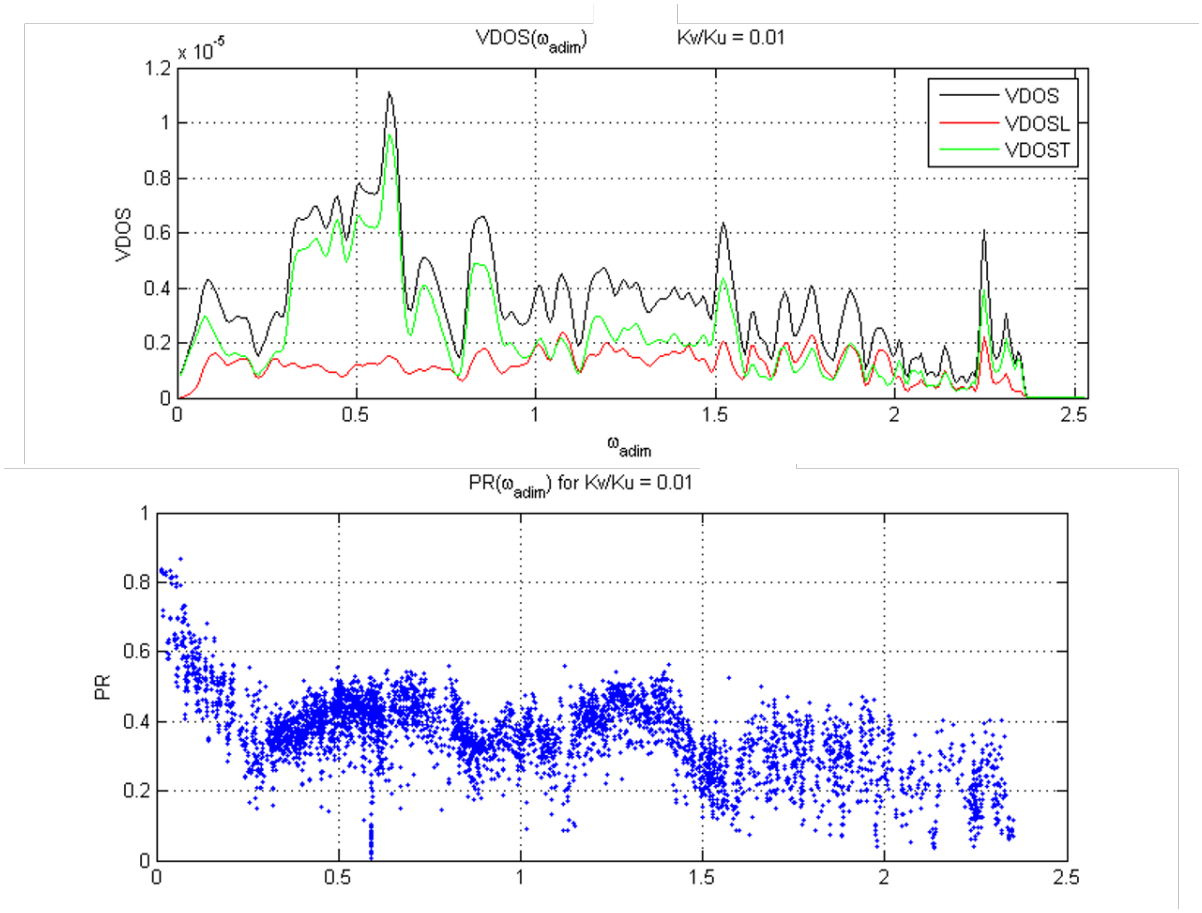

FIGURE 10 – top :Complete, Longitudinal and Transverse VDOS for the 4th approximant of Penrose lattice with $\frac{K_v}{K_u} = 0.01$. bottom : PR for the same structure.

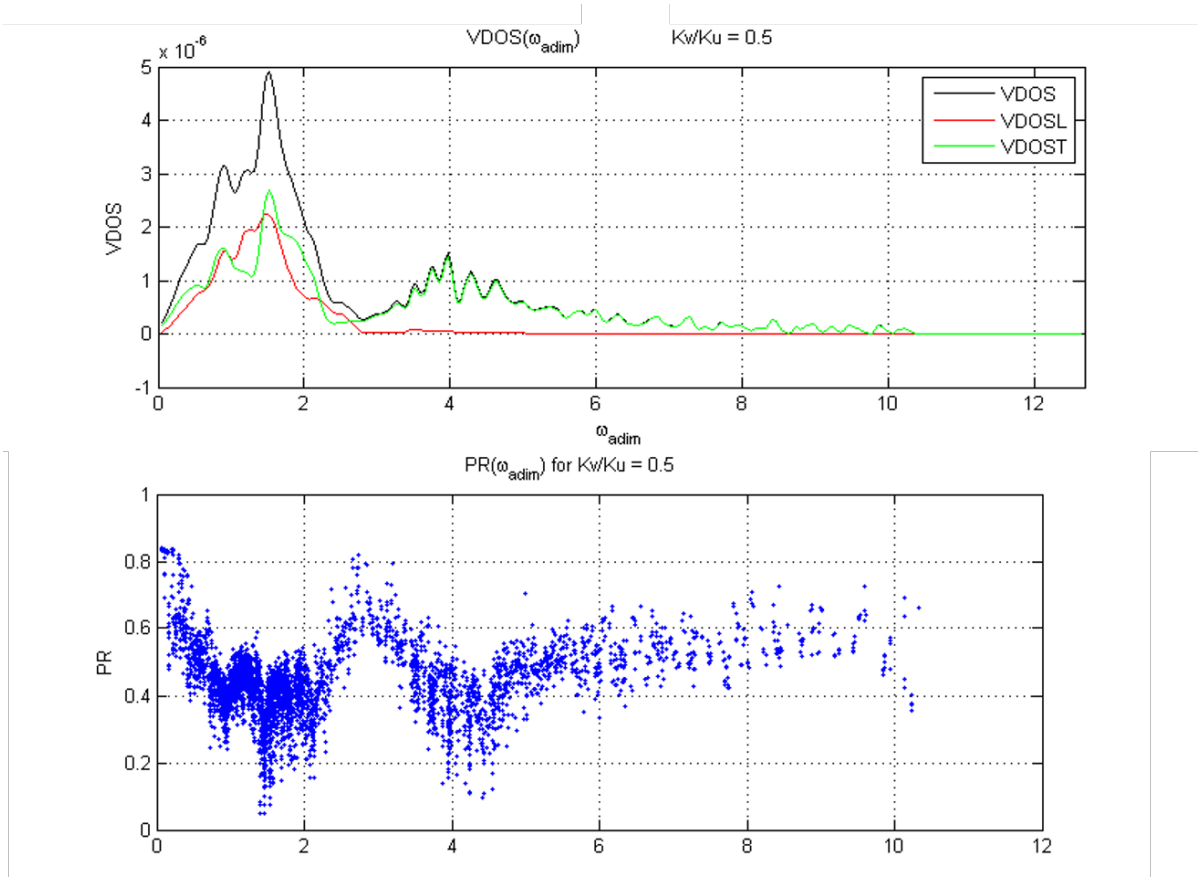

FIGURE 11 – top :Complete, Longitudinal and Transverse VDOS for the 4th approximant of Penrose lattice with $\frac{K_v}{K_u} = 0.5$. bottom : PR for the same structure.

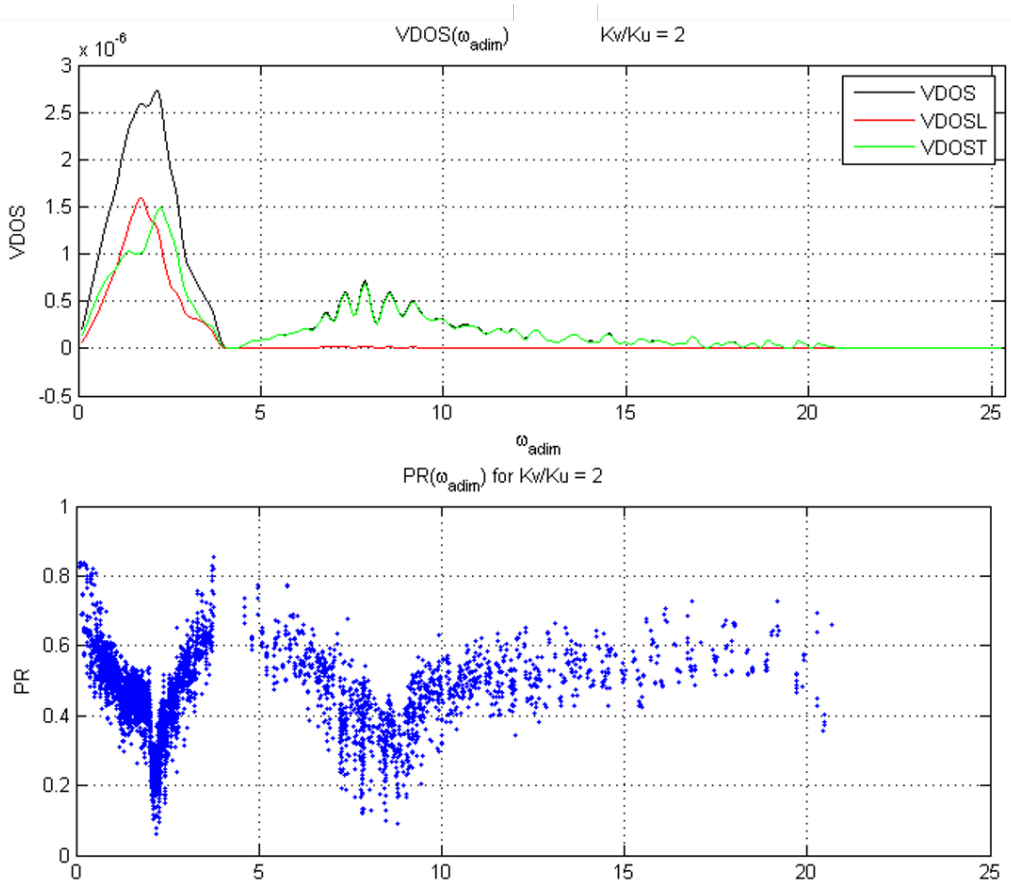

FIGURE 12 – top :Complete, Longitudinal and Transverse VDOS for the 4th approximant of Penrose lattice with $\frac{K_v}{K_u} = 2$. bottom : PR for the same structure.

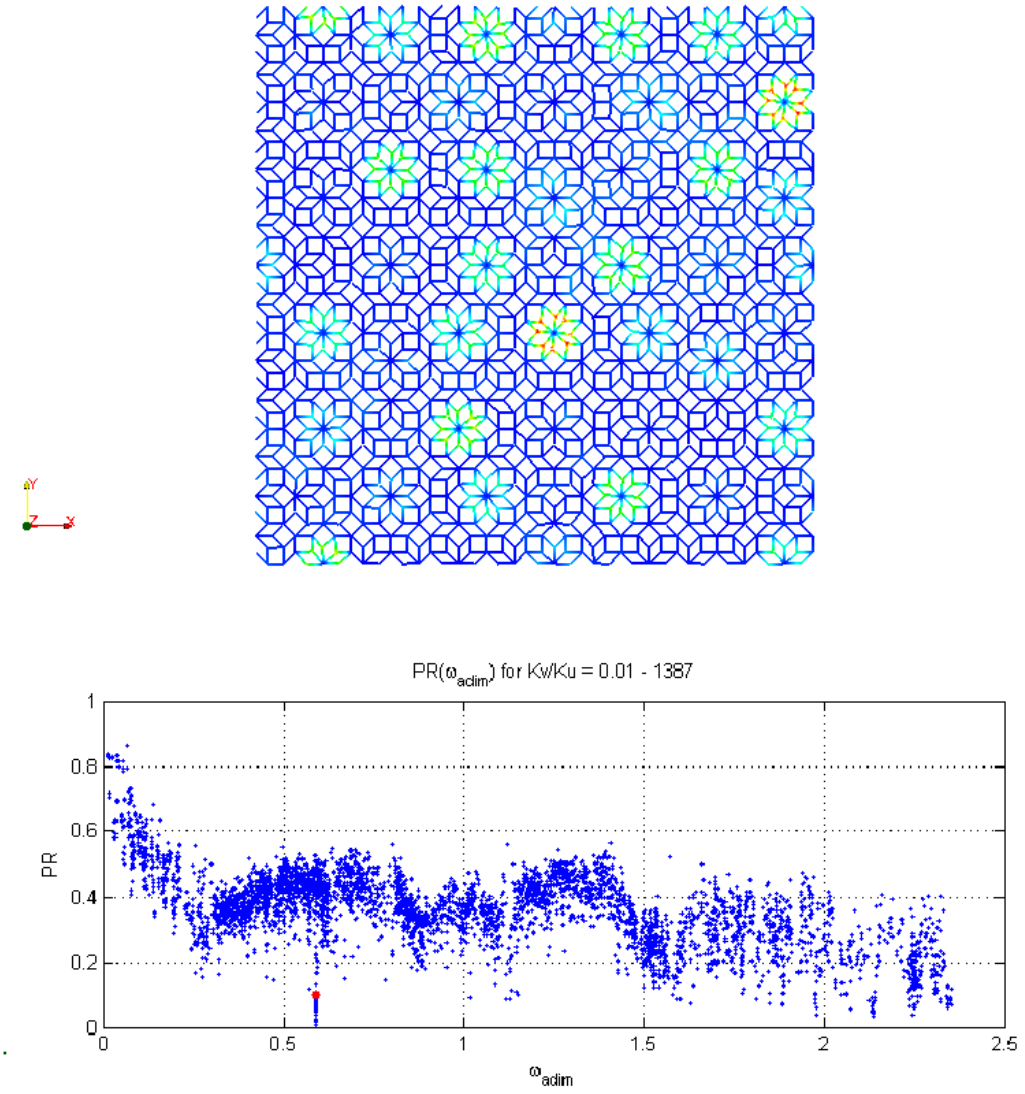

FIGURE 13 – Deformed lattice and PR (full PR in blue, corresponding mode in red) of the 1387th mode for the 4th approximant of Penrose lattice with $\frac{K_v}{K_u} = 0.01$.

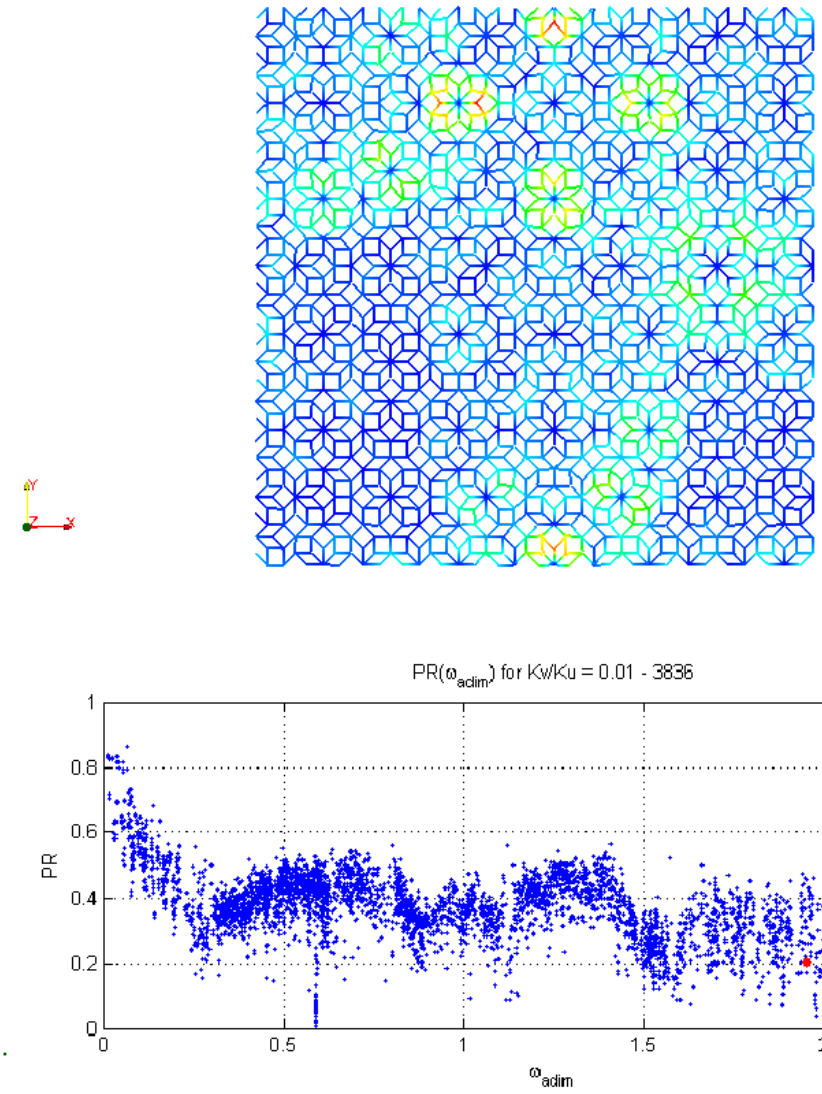

FIGURE 14 – Deformed lattice and PR (full PR in blue, corresponding mode in red) of the 3836th mode for the 4th approximant of Penrose lattice with $\frac{K_v}{K_u} = 0.01$.

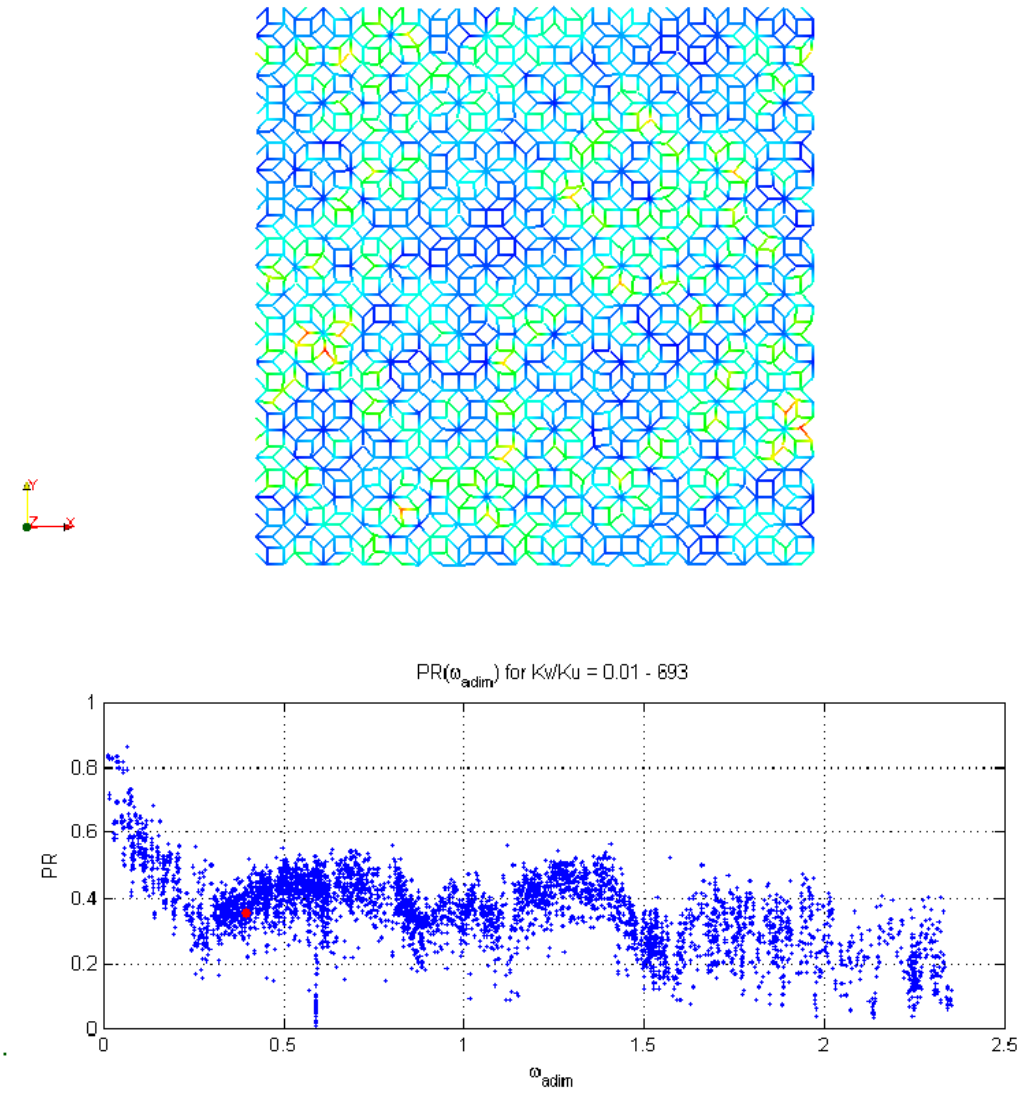

FIGURE 15 – Deformed lattice and PR (full PR in blue, corresponding mode in red) of the 693th mode for the 4th approximant of Penrose lattice with $\frac{K_v}{K_u} = 0.01$.

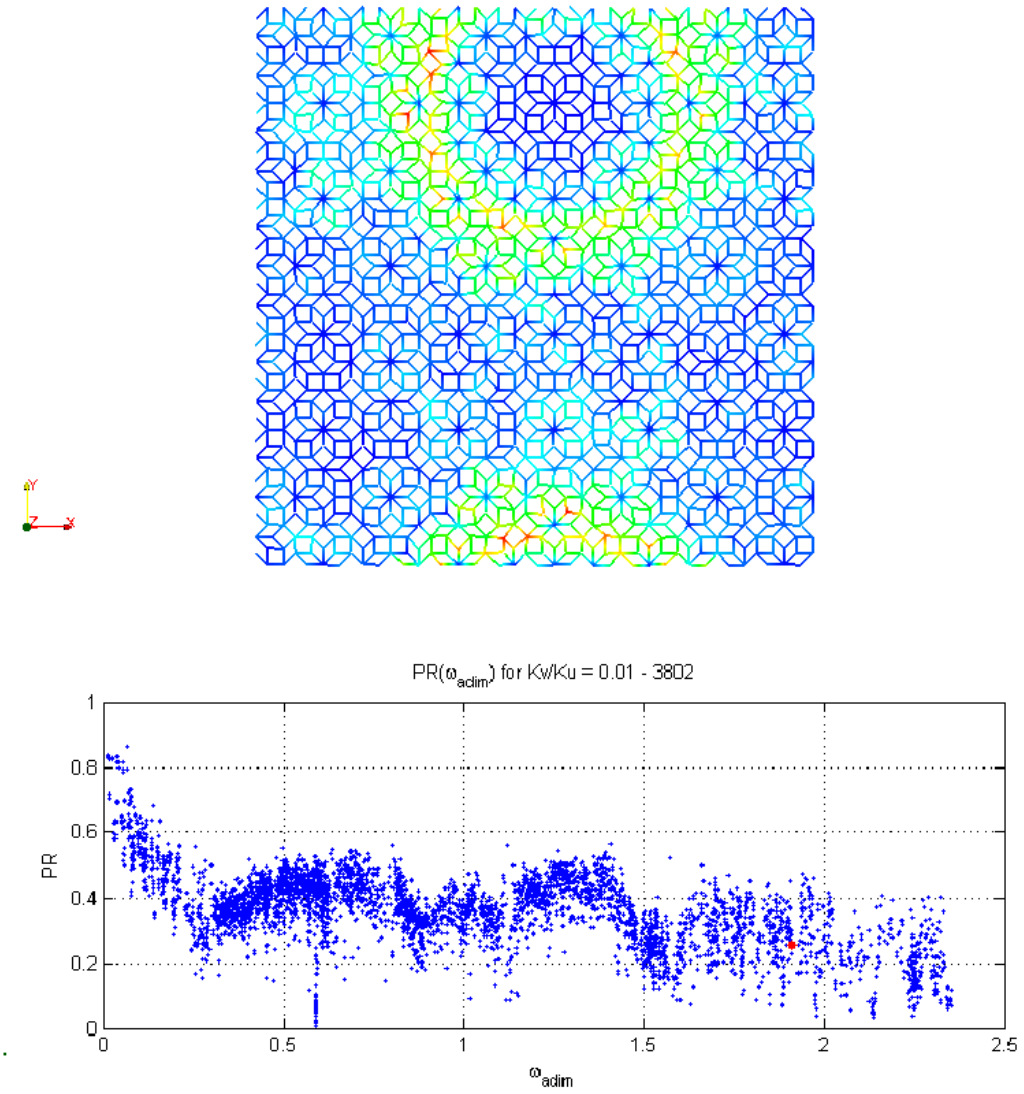

FIGURE 16 – Deformed lattice and PR (full PR in blue, corresponding mode in red) of the 3802 th mode for the 4th approximant of Penrose lattice with $\frac{K_v}{K_u} = 0.01$.

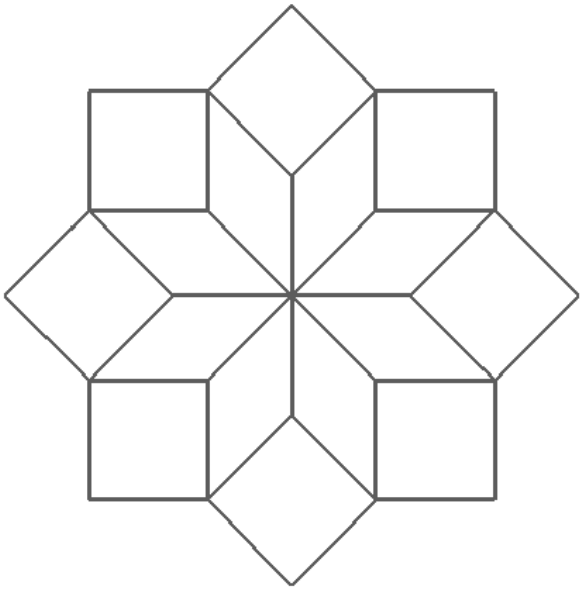

FIGURE 17 – Star structure.

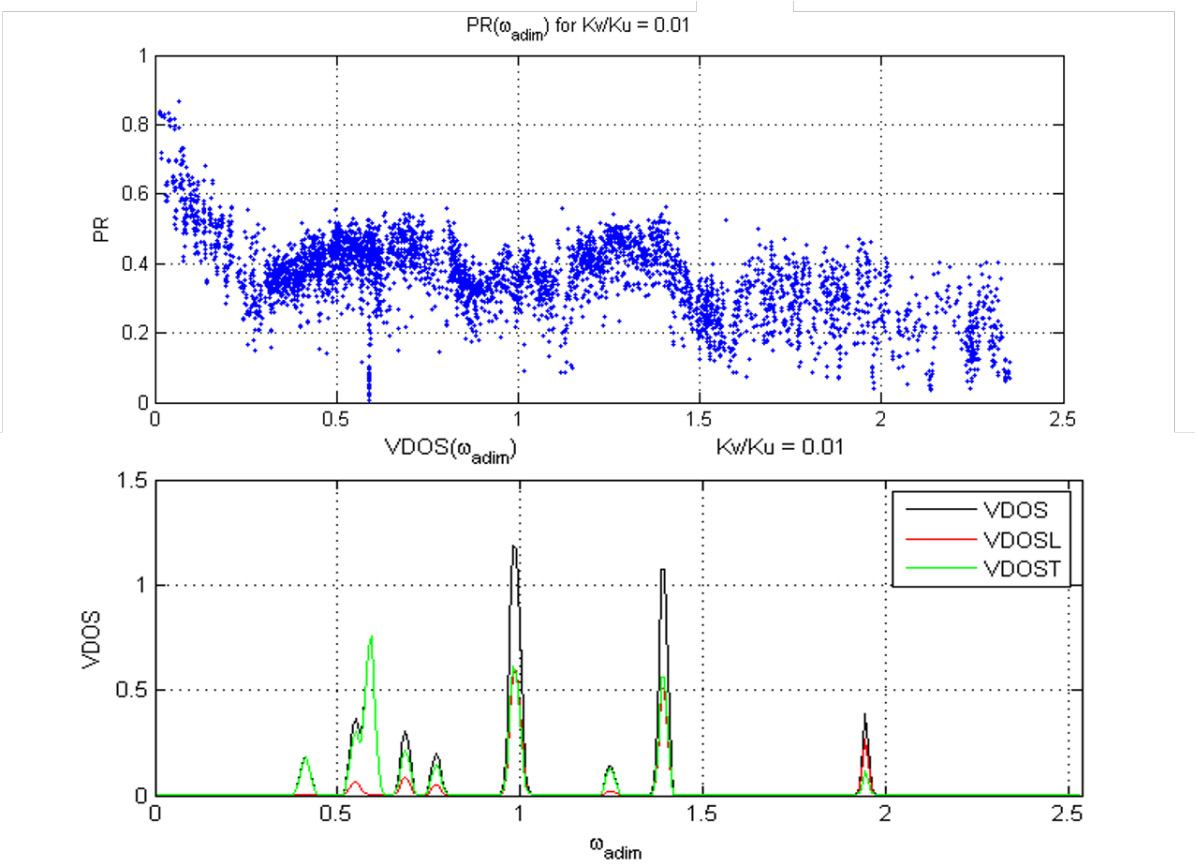

FIGURE 18 – VDOS of the star superposed to the PR of the 4th approximant of Penrose lattice with $\frac{K_v}{K_u} = 0.01$..

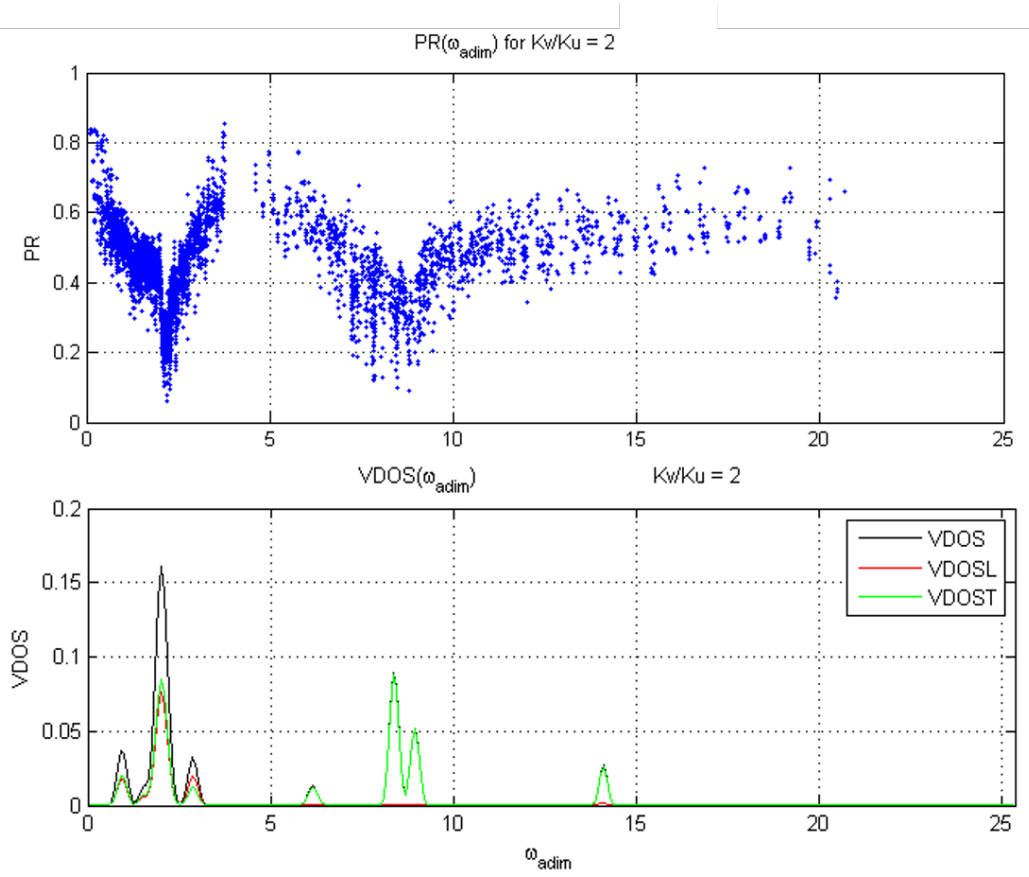

FIGURE 19 – VDOS of the star superposed to the PR of the 4th approximant of Penrose lattice with $\frac{K_v}{K_u} = 2$.

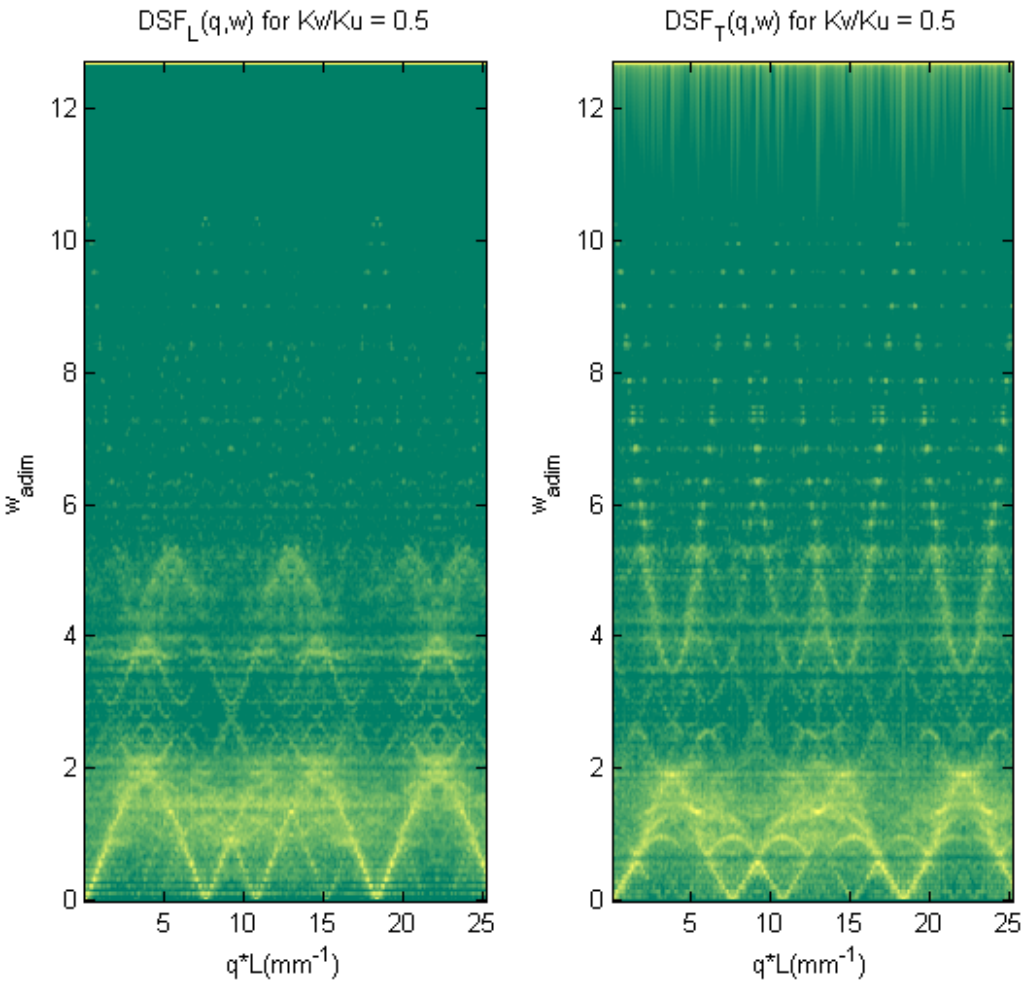

FIGURE 20 – Log of DSF for the 4th approximant of Penrose lattice with $\frac{K_v}{K_u} = 0.5$.

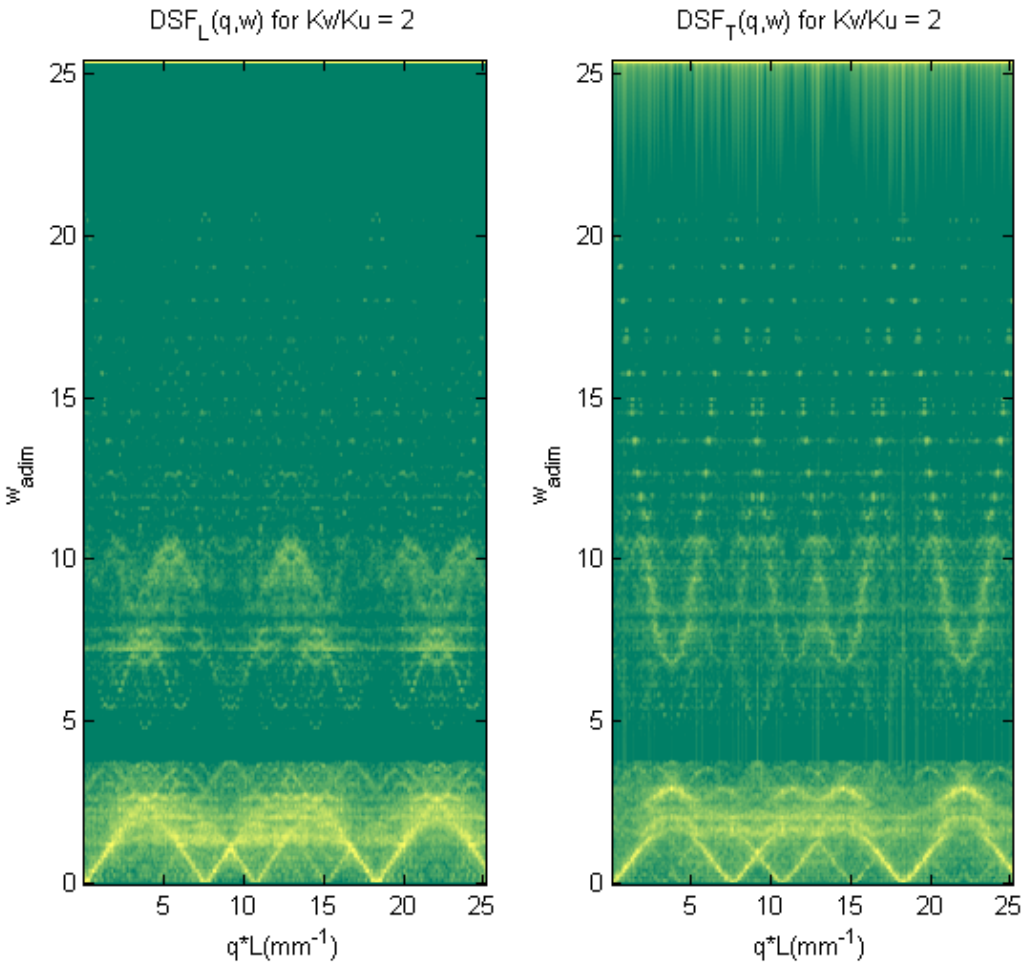

FIGURE 21 – log of DSF for the 4th approximant of Penrose lattice with $\frac{K_v}{K_u} = 2$.